REVIEWS

Journal of Semiconductors
(2023) 44, 101301
doi: 10.1088/1674-4926/44/10/101301

Fundamentals and applications of photonic waveguides with bound states in the continuum

Zejie Yu[1, 3, 4, †], He Gao[1], Yi Wang[2], Yue Yu[2], Hon Ki Tsang[2], Xiankai Sun[2], and Daoxin Dai[1, 3, 4, 5]

[1]Centre for Optical and Electromagnetic Research, State Key Laboratory for Modern Optical Instrumentation, Zhejiang Provincial Key Laboratory for Sensing Technologies, International Research Center for Advanced Photonics, College of Optical Science and Engineering, Zhejiang University, Hangzhou 310058, China

[2]Department of Electronic Engineering, The Chinese University of Hong Kong, Shatin, New Territories, Hong Kong SAR, China

[3]Jiaxing Key Laboratory of Photonic Sensing & Intelligent Imaging, Jiaxing 314000, China

[4]Intelligent Optics & Photonics Research Center, Jiaxing Research Institute Zhejiang University, Jiaxing 314000, China

[5]Ningbo Research Institute, Zhejiang University, Ningbo 315100, China

Abstract: Photonic waveguides are the most fundamental element for photonic integrated circuits (PICs). Waveguide properties, such as propagation loss, modal areas, nonlinear coefficients, etc., directly determine the functionalities and performance of PICs. Recently, the emerging waveguides with bound states in the continuum (BICs) have opened new opportunities for PICs because of their special properties in resonance and radiation. Here, we review the recent progress of PICs composed of waveguides with BICs. First, fundamentals including background physics and design rules of a BIC-based waveguide will be introduced. Next, two types of BIC-based waveguide structures, including shallowly etched dielectric and hybrid waveguides, will be presented. Lastly, the challenges and opportunities of PICs with BICs will be discussed.

Key words: photonic waveguide; bound states in the continuum; integrated photonics

Citation: Z J Yu, H Gao, Y Wang, Y Yu, H K Tsang, X K Sun, and D X Dai, Fundamentals and applications of photonic waveguides with bound states in the continuum[J]. *J. Semicond.*, 2023, 44(10), 101301. https://doi.org/10.1088/1674-4926/44/10/101301

1. Introduction

Photonic integrated circuits (PICs) can enable systems to operate with a large bandwidth, high speed, low power consumption, and high thermal stability, and have the potential to revolutionize the future technologies used in multidisciplinary areas such as high-speed communication[1, 2], energy-efficient computating[3, 4], quantum information processing and communications[5, 6], and precise metrology[7, 8]. Integrated optical waveguides are the fundamental element for constructing PICs, and are of critical importance. Key characteristics of a waveguide include their effective refractive index (RI), RI contrast between the guide and cladding regions, waveguide sidewall roughness, waveguide feature size, nonlinear coefficients, loss, and optical dispersion and these directly influence the performance and functionalities in PICs. For example, the high integration density of PICs requires the use of waveguides with high RI and high RI contrast to realize small modal areas, weak coupling between closely positioned adjacent waveguides, and a small bending radius. Waveguides with low propagation losses are often a key requirement for high-performance PICs and are an essential prerequisite for the integration of a large number of devices on a chip. Strong light–matter interaction in applications of optical emission[9–12], detection[13, 14], and wavelength conversion[15–17] require waveguides with large nonlinear coefficients, small modal areas, low loss, etc.

A variety of waveguides, as shown in Fig. 1, have been widely explored in different material platforms[19–22]. A strip waveguide is the most popular waveguide with characteristics such as simple structures, small modal area, large RI contrast, etc. Although the strip waveguide offers high performance for most applications, there are some circumstances when other waveguide structures are needed. For example, a ridge waveguide can have a smaller optical field overlap with the shallowly etched sidewalls than strip waveguides, thus achieving lower propagation loss. Subwavelength grating structures can be used for waveguides and offer an additional degree of freedom for engineering the effective RI, birefringence, and dispersion, and may be used to design devices with wider working bandwidths[23]. Photonic crystal waveguides with engineered band diagrams could realize unusual phenomena such as sharp bending[24], slow light[25], and topological protection[26]. Plasmonic waveguides confining light into the deep subwavelength region is a good platform to study nonlinear light–matter interactions[27, 28]. Hybrid waveguides integrating different materials can realize active and passive devices on a single chip[18, 29].

Bound states in the continuum (BICs) were first mathematically proposed in 1929 by von Neumann and Wigner[30]. Solved from the Schrödinger equation, a typical potential well only supports a wave with eigenenergy below the potential well, and the wave is called a bound state of the potential well. Other states with eigenenergy above the potential well are known as continuous states, which cannot be effectively confined and will spread to infinity. A bound state with eigenenergy above the potential well will suffer large leakage loss because of the interaction with radiation waves. BIC

Correspondence to: Z J Yu, zjyu@zju.edu.cn
Received 15 MARCH 2023; Revised 9 MAY 2023.

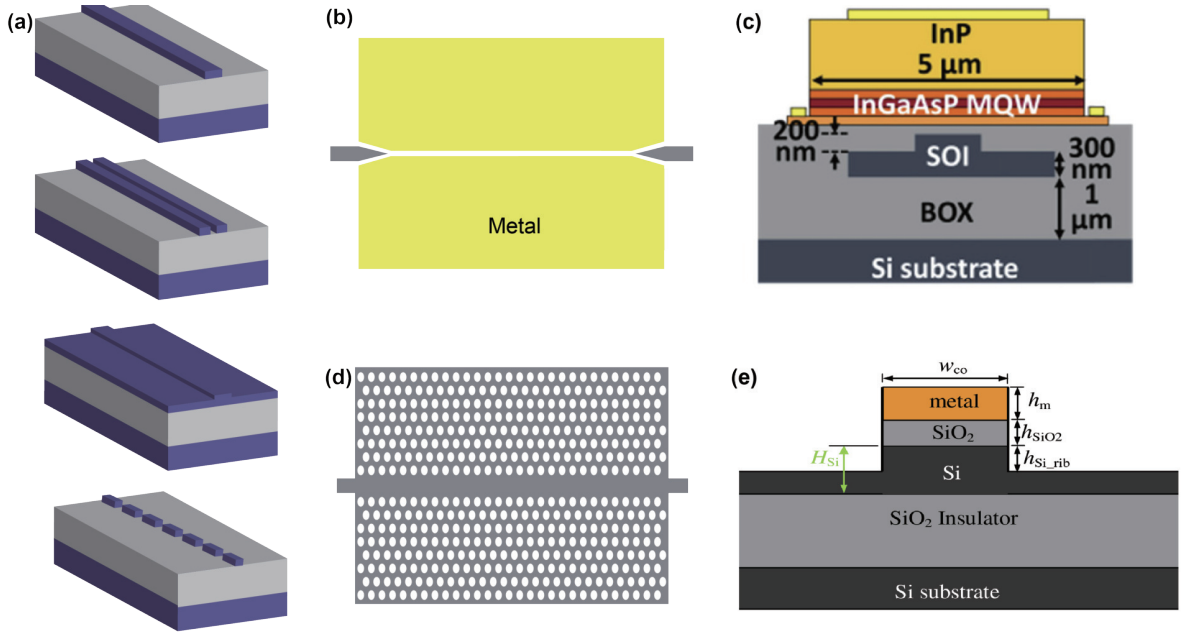

Fig. 1. (Color online) (a) Strip, slot, ridge, and subwavelength waveguides. (b) A plasmonic slot waveguide. (c) A hybrid waveguide[18]. Copyright 2016, The Optical Society. (d) A photonic crystal waveguide. (e) A hybrid plasmonic cap waveguide[28]. Copyright 2009, The Optical Society.

is just an exception that has eigenenergy above the potential well but is perfectly confined in the continuous spectrum without any loss. Even though the original proposal constructing an artificial quantum well to support an electronic state with energy that falls above the continuum threshold was never practically realized[31], BICs are a general wave phenomenon that can be explored in other systems such as electromagnetic[32–45] and acoustic[46–50] waves. For example, BICs can be obtained in photonics using the similarity between the Schrödinger equation and the Helmholtz equation, the refractive index n of a material determines the potential for photons as $-n^2k^2_0$, where k_0 is the light's wavenumber in the vacuum. Recently, photonics become a hot platform to explore the background physics of BICs because of the advancement of micro/nano-fabrication technology. Different types of BICs have been observed in different kinds of photonic structures including supercavities[43], photonic crystals[51], metasurface[52, 53], photonic waveguide arrays[44, 54], hybrid waveguides[55, 56], plasmonic metagrating[57], etc.

Among the different kinds of waveguides in Fig. 1, most of them only support optical modes that do not couple with leakage modes. The supported mode is recognized as a bound mode of the corresponding waveguide. In recent years, a new type of waveguide supporting BICs gradually attract attention due to their special optical properties. Optical modes belonging to the category of BICs in waveguides can propagate without any leakage loss even though they coexist and couple with leaky continuous modes[56, 58]. The waveguide with BICs has brought new chances to PICs and many applications have been demonstrated such as cavities[56, 58, 59], filters[60], modulations[55, 59, 61], and detections[62, 63]. In this paper, a review is given of the recent progress of waveguides with BICs, and fundamentals, applications, challenges, and opportunities will be introduced.

2. Fundamentals of a waveguide with BICs

Generally, modal profiles, propagation loss, and propagation speed (inversely proportional to group RI) are three crux features to characterize light properties in a waveguide. A slab waveguide as shown in Fig. 2(a) consists of three layers of materials with RIs of n_1, n_2, and n_3, respectively, where n_2 is larger than both n_1 and n_3. All RIs n_1, n_2, and n_3 are assumed to be real numbers because negligible material absorption is highly desired for PIC applications. The optical properties of a passive waveguide can be solved by the passive Helmholtz equation as

$$\nabla^2 A(x,y,z) - \frac{n(x,y,z)}{c} A(x,y,z) = 0, \quad (1)$$

where n and c denote the RI of the material and light speed in the vacuum, respectively. Solved modal profiles for both polarizations are plotted as solid (p-polarization) and dashed (s-polarization) lines in Fig. 2(a), where s polarization with the electrical field perpendicular to the interface of two materials has an effective RI of n_s and p polarization with the electrical field parallel to the interface of two materials has an effective RI of n_p. n_p is usually larger than n_s because the higher RI material concentrates more p-polarized light than s-polarized light. The propagation loss of both s- and p-polarized light can be neglected by assuming zero roughness at the interface of two materials.

A strip waveguide as shown in Fig. 2(b) is more practical than a slab waveguide in real applications. In order to solve the optical properties of the strip waveguide, it can be divided into three regions and the central region can be approximated as a slab waveguide. In the side regions, the effective RI of both s- and p-polarized light can be approximated as n_1. In terms of the central region, as discussed for the slab waveguide, the effective RIs of s- and p-polarized light can be approximated as n_s and n_p, respectively. The solid (p-polarized) and dashed (s-polarized) lines in Fig. 2(b) plot the effective RI distributions for s- and p-polarized light, respectively. It should be noted that only the TE (TM) mode can be solved from the $p(s)$-polarized effective-RI distribution because the polarization of light has been assumed when plot-

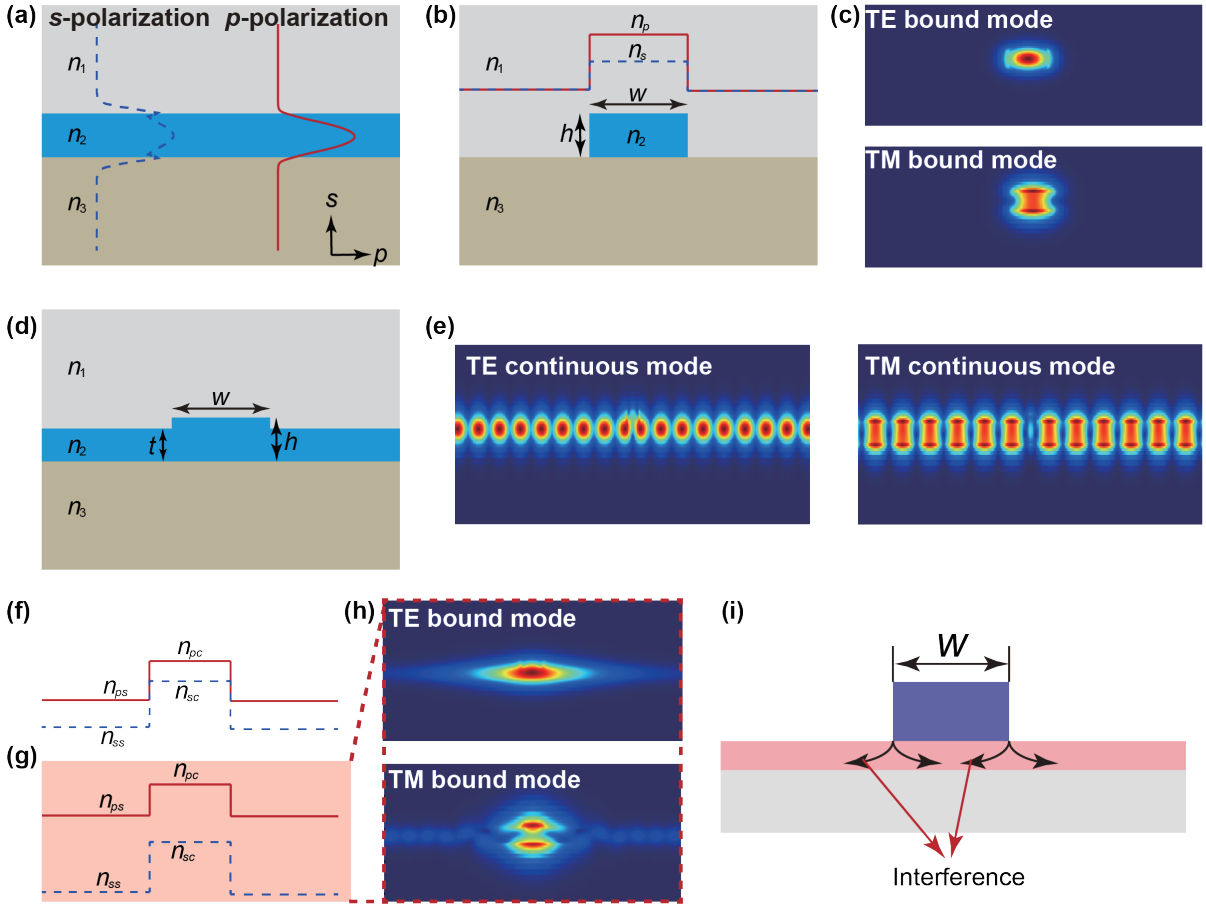

Fig. 2. (Color online) (a) A slab waveguide and its *s*- and *p*-polarized modal profiles. (b) A strip waveguide with its RI distributions of both *s* and *p* polarizations. (c) Modal profiles $|\boldsymbol{E}|$ of the TE and TM modes in a strip waveguide. (d) A ridge waveguide. (e) Modal profiles $|\boldsymbol{E}|$ of TE and TM continuous modes. The RI distributions of the ridge waveguide with $n_{sc} > n_{ps}$ (f) and $n_{sc} < n_{ps}$ (g). (h) Modal profiles of the TE and TM modes in a thin-ridge waveguide with $n_{sc} < n_{ps}$. (i) Schematically illustration of leakage channels.

ting the effective RI distributions. Fig. 2(c) shows the solved modal profiles $|\boldsymbol{E}|$ of the TE and TM modes, where the TE mode usually has a larger effective RI than that of the TM mode because the width w of the waveguide usually is larger than the height h.

Fig. 2(d) shows a ridge waveguide with shallowly etched sidewalls. Like a strip waveguide, it can also be divided into three regions to solve the optical properties. Each region of the ridge waveguide can be seen as a slab waveguide. The central and side regions have effective RIs of n_{sc} (n_{pc}) and n_{ss} (n_{ps}) for *s*(*p*)-polarized light, where n_{sc} (n_{ss}) < n_{pc} (n_{ps}) and n_{sc} (n_{pc}) > n_{ss} (n_{ps}). Regarding modal properties in the ridge waveguide, at first, there are many TE (TM) continuous modes with effective RIs smaller than n_p (n_s) existing in the slab as shown in Fig. 2(e). These modes extend to the infinite in the lateral direction of the waveguide so that suffer large leakage loss. In terms of the guided modes, the TE and TM modes with effective RIs of n_{TE} and n_{TM} can be obtained, where $n_{ps} < n_{TE} < n_{pc}$ and $n_{ss} < n_{TM} < n_{sc}$ as analyzed above. In view of that, the effective RI of *s*-polarized light at the side regions will decrease with the etching depth, so the TE and TM modal evolution mechanism in the ridge waveguide can be divided into two cases according to the relative value between n_{sc} and n_{ps}. Fig. 2(f) plots the effective RIs distributions of the ridge waveguide with $n_{sc} > n_{ps}$, which is similar to the condition of the strip waveguide. Fig. 2(g) plots the case of $n_{sc} < n_{ps}$, which indicates that the RI distribution of *s*-polarized light is below the RI distribution of *p*-polarized light. Given the fact that the RI contrast for the TE polarization is quite small in a thin-ridge waveguide, the TE mode (Fig. 2(h)) has a weak confinement that is not suitable for constructing compact integrated devices. In addition, despite *s*-polarization has a relatively large RI contrast because the discontinuities of the electric field at the up and down boundaries make *s*-polarization more sensitive to the waveguide thickness, the TM mode falls in the TE continuous spectrum so that a TE continuous mode with the same effective RI as n_{TM} can be found. Considering the TM mode in the ridge waveguide actually is a quasi-TM mode that contains both *s* and *p* polarizations, the TM mode as shown in Fig. 2(h) will couple with the leaky TE continuous modes so that suffers large propagation loss.

Obtaining a BIC is a solution to overcome the leakage loss of the TM mode in the TE continuous spectrum if taking the thin-ridge waveguide into PIC applications. As shown in Fig. 2(i), the leakage channels of the TM bound mode in the ridge waveguide are at the corners and at each corner both left- and right-going leakages exist. Leakages with the same direction will interfere with each other and effective leakage can be reduced to zero when destructive interferences happen, enabling zero propagation loss for the TM mode. For a straight waveguide, the interference can be simply controlled by changing the width of the ridge waveguide, the propagation length can be expressed as $L \propto w^2/\sin^2(k_p w/2)$[58], with k_p the *p* component of the wave vector of the TE continu-

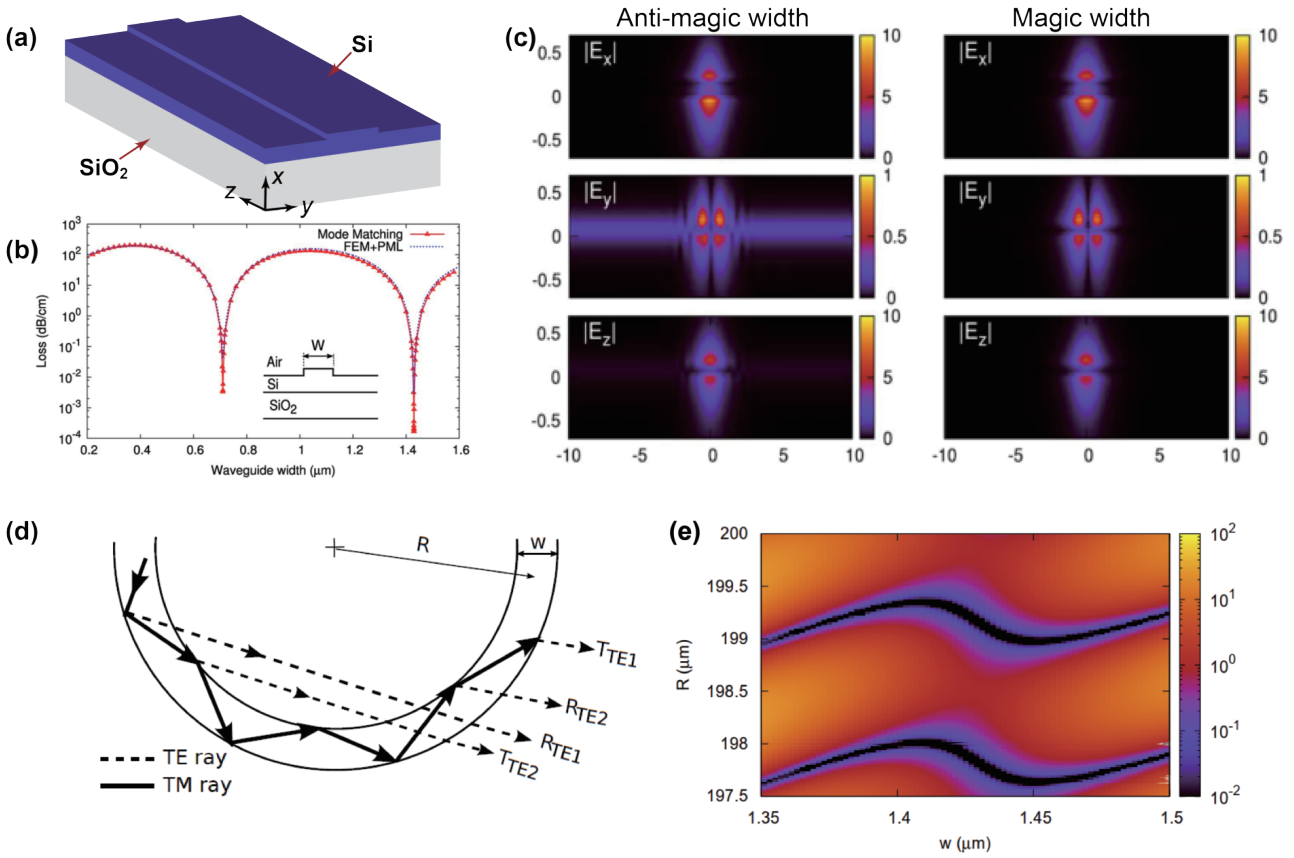

Fig. 3. (Color online) (a) Schematically illustration of a thin-ridge silicon waveguide. (b) The propagation loss of the TM mode as a function of the waveguide width[72]. Copyright 2009, IEEE. (c) Modal profiles of the TM mode at waveguides with "magic width" and "anti-magic width"[72]. Copyright 2009, IEEE. (d) Planar view and modal coupling diagram of a bend thin-ridge waveguide[81]. Copyright 2010, The Optical Society. (e) The propagation loss of the TM mode in a bent waveguide as a function of the waveguide width and radius[81]. Copyright 2010, The Optical Society.

ous mode. For a bent waveguide, the interference depends on both waveguide width w and bending radius R, the propagation loss can be briefly expressed as $\propto|J_q(nk_0R) - \xi Jq(nk_0(R-wb))|$[58], where J_q is the qth Bessel function with q the azimuthal mode number. The waveguide with parameters supporting negligible propagation loss can be called a BIC waveguide and the corresponding guided TM mode is a BIC.

3. Silicon waveguides with BICs

Silicon ridge waveguides with BICs have been widely and thoroughly investigated on a silicon-on-insulator platform[64–80]. According to the propagation direction of light, the working mechanism of BICs can be categorized into two types: one is that light propagates along a silicon ridge waveguide and the other is that light propagates with a certain angle between a silicon ridge waveguide.

Light propagating along a silicon thin-ridge waveguide. A shallowly etched waveguide on an SOI platform as shown in Fig. 3(a) is a typical platform to study the case of light propagating along a silicon thin-ridge waveguide. Despite semi-analytical mode-matching methods have been developed to solve the leakage behavior of the TM mode[72], numerical simulation is the most widely adopted method to accurately analyze leakage by solving eigenmodes in the waveguide cross section, where the propagation loss can be evaluated from the imaginary part of the solved eigenmodal effective RI. The finite element method with absorption boundaries e.g., perfectly matched layer boundaries is a typical approach to obtain effective RIs. The simulated leakage loss of the TM mode as a function of the waveguide width is presented in Fig. 3(b), where the propagation loss of the TM mode varies periodically with the waveguide width. These special widths for minimum or maximum propagation loss were called "magic widths" or "anti-magic widths". Moreover, the TM mode at the waveguide with magic or anti-magic width can be recognized as a BIC or anti-BIC. Fig. 3(c) shows vectorial components of the electric field distributions of the guided modes for a waveguide with "magic width" and "non-magic width", respectively. Comparing the components, despite the *s*-polarized components being effectively confined by the thin-ridge waveguide, a significant *p*-polarized component with field values approximately ten times smaller than the *s*-polarized component exhibits strong radiation at the waveguide with a "non-magic" width. The leakage behavior was also explored in a bent thin-ridge waveguide[81] as shown in Fig. 3(d). The simulated results in Fig. 3(e) reveal that the propagation loss is sensitive to both waveguide radius and width, the interplay between waveguide radius and width is nontrivial. The lateral leakage can be significantly reduced with "magic parameters" but cannot be reduced to zero due to the impact of the conventional bending loss.

The lateral leakage behaviors in a ridge waveguide were experimentally investigated on an SOI platform[66]. The lateral leakage was proved by scattering radiated light into free

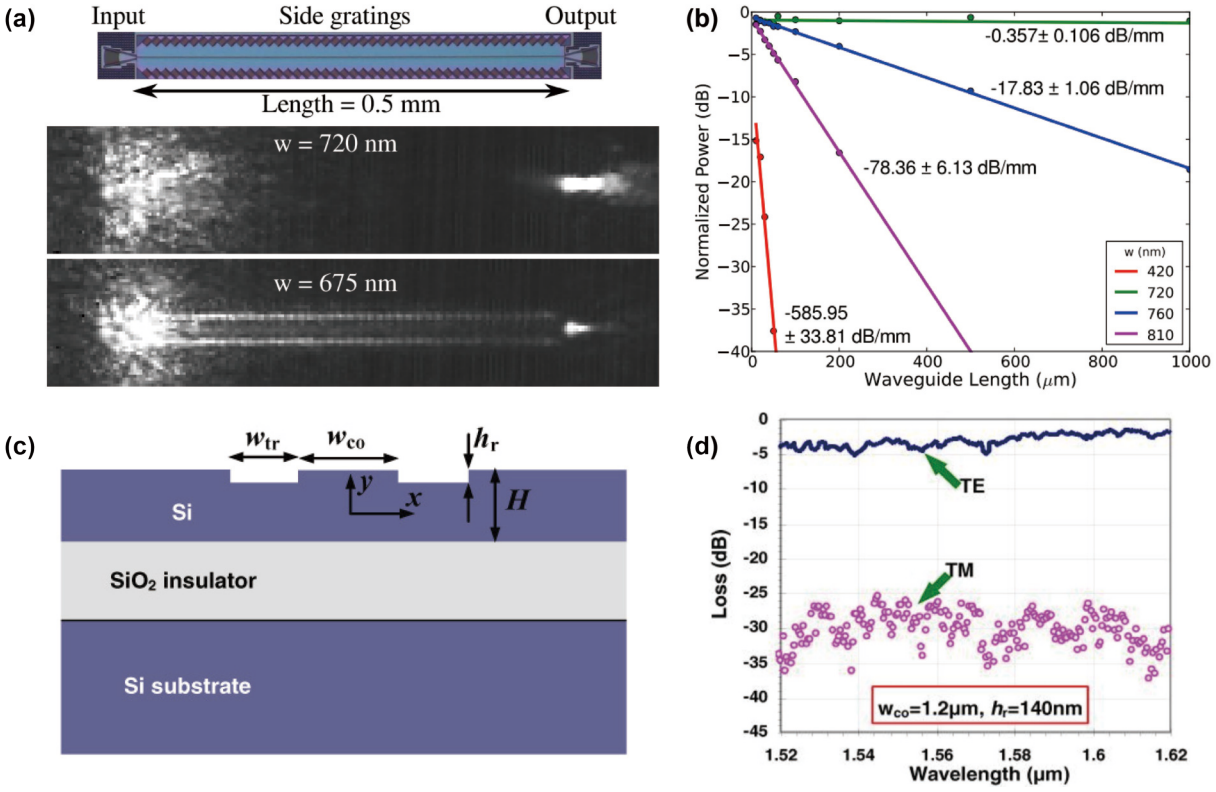

Fig. 4. (Color online) (a) A fabricated silicon thin-ridge waveguide and the scattering field views of waveguides with "magic width" and "non-magic width"[66]. Copyright 2016, IEEE. (b) The measured propagation loss of the waveguide with different widths[66]. Copyright 2016, IEEE. (c) Modal profiles of the TE and TM modes in a waveguide with "anti-magic" structural parameters[82]. Copyright 2010, The Optical Society. (d) The measured results for the transmissions of the TE and TM modes[82]. Copyright 2010, The Optical Society.

space with the assistance of side gratings as shown in Fig. 4(a). The waveguide with a "magic width" has an image with darkness, presenting clear evidence of the suppression of lateral leakage, while the waveguide with a "non-magic width" has an image with excitation decreasing with distance from the input, presenting clear evidence of lateral leakage behavior in the ridge. Fig. 4(b) shows the propagation loss as a function of waveguide width at the wavelength of 1550 nm, indicating the minimum propagation loss of 0.357 dB/mm.

A simple and broadband polarizer as shown in Fig. 4(c) was proposed based on the distinct propagation loss between the TE and TM modes of a thin-ridge waveguide on an SOI platform[82]. The theoretical calculation shows that the loss of the TE mode can be very low while at the same time the TM mode has a very large leakage loss when the waveguide with an "anti-magic" width. The polarizer is fabricated on an SOI wafer with a 700-nm-thick top layer silicon and then characterized by using a free-space optical system. As shown in Fig. 4(d), the measured extinction ratio is as high as 25 dB over a 100 nm wavelength range for a 1-mm-long polarizer.

Angled propagation across a silicon thin-ridge waveguide. According to the BIC formation mechanism of coupling between the TE continuous and TM modes, similar to the condition that TM mode propagating in a ridge waveguide, photonic BICs can also be explored when TE continuous modes incident on a silicon thin-ridge waveguide with a certain angle as shown in Fig. 5(a)[77]. Under the oblique incidence of a *p*-polarized light on the thin-ridge waveguide, BICs can be observed at the reflectance and transmittance spectra, featured as high-*Q* resonances. The BICs or resonances highly depend on the incident angle and waveguide width because of the phase-matching requirement of coupling. A theoretical model was developed to explain these optical properties based on the coupled-mode method, not only proving the existence of BICs but also predicting their corresponding locations[77]. The accuracy of the theoretical model was verified by the aperiodic rigorous coupled-wave analysis method. The phenomenon was experimentally observed based on an SOI platform as shown in Fig. 5(b) using the foundry-compatible fabrication process[76]. A single-mode waveguide launches a slab waveguide mode by adiabatically expanding the width. The slab mode is collimated by a parabolic reflector and then propagates to a 650-nm-wide ridge resonator under an angle of 52.2°. The transmitted light is focused into the right single-mode waveguide by another parabolic reflector. A single and strong resonant dip is observed at the wavelength of 1539 nm with a *Q* factor of 520.

The BIC-enabled ridge resonance has also been observed in a metagrating-assisted waveguide as shown in Fig. 5(c)[83], where the launched TE continuous mode is perpendicular with the ridge waveguide. By satisfying the phase-matching condition through the assistance of shallow-ridge metagrating embedded in the silicon slab waveguide, the input slab mode can be coupled into the resonant TM mode, which can be further transformed into the supercavity mode by utilizing the intra-waveguide Fabry–Perot interference. The fabricated metagrating operating near the supercavity regime with an experimentally observed high-quality factor ≈ 5200

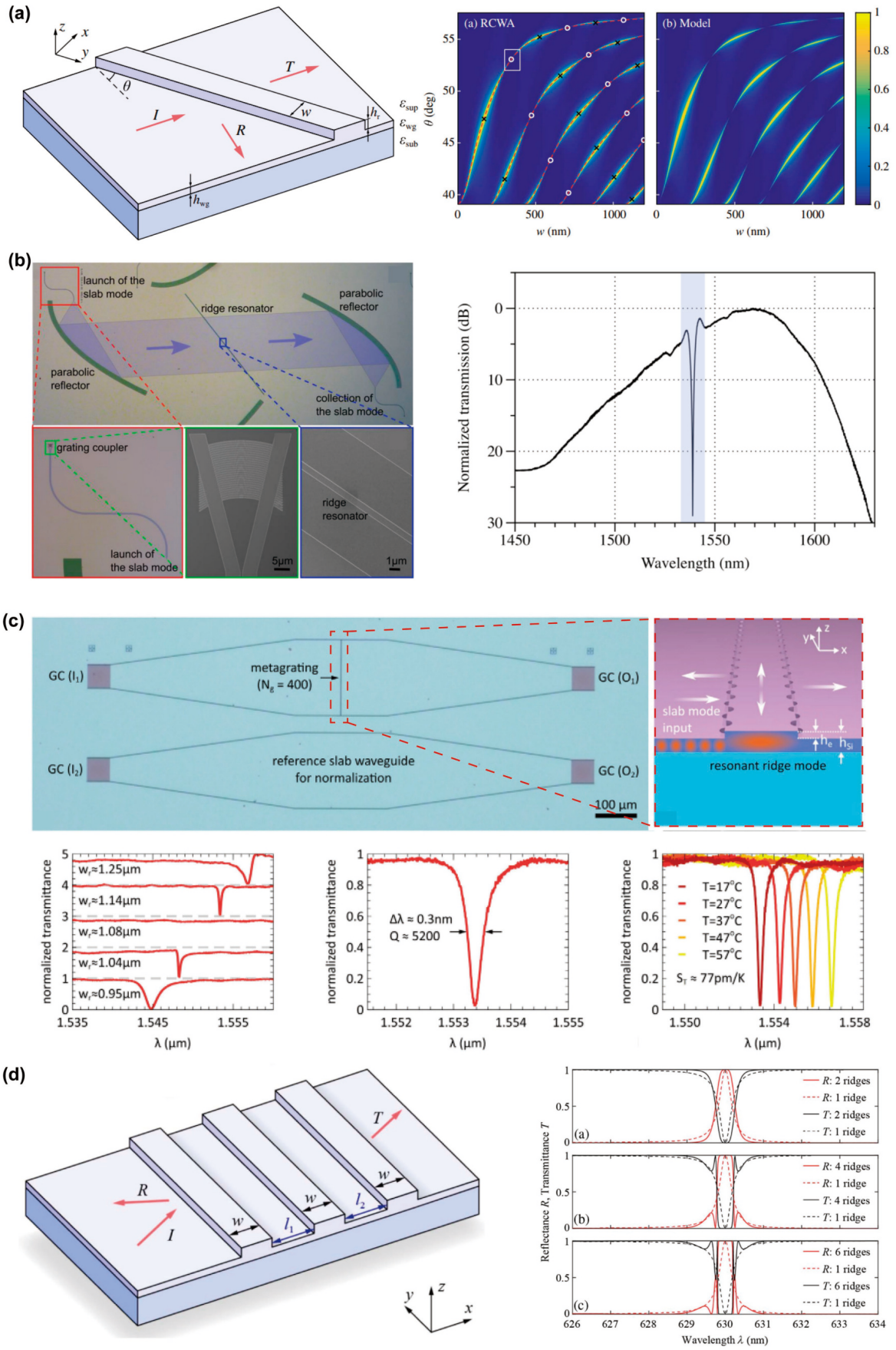

Fig. 5. (Color online) (a) Schematic illustration of a silicon thin-ridge waveguide supporting BIC resonances and its simulated transmission spectra as a function of waveguide width and incident angle[77]. Copyright 2018, Chinese Laser Press. (b) A fabricated silicon waveguide supporting BIC resonances and its measured resonance[76]. Copyright 2019, John Wiley & Sons. (c) A fabricated metagrating waveguide and its measured BIC resonance for applications in sensing[83]. Copyright 2020, John Wiley & Sons. (d) A flat-top filter based on BIC waveguides and its simulated transmission and reflection spectra[60]. Copyright 2019, Chinese Laser Press.

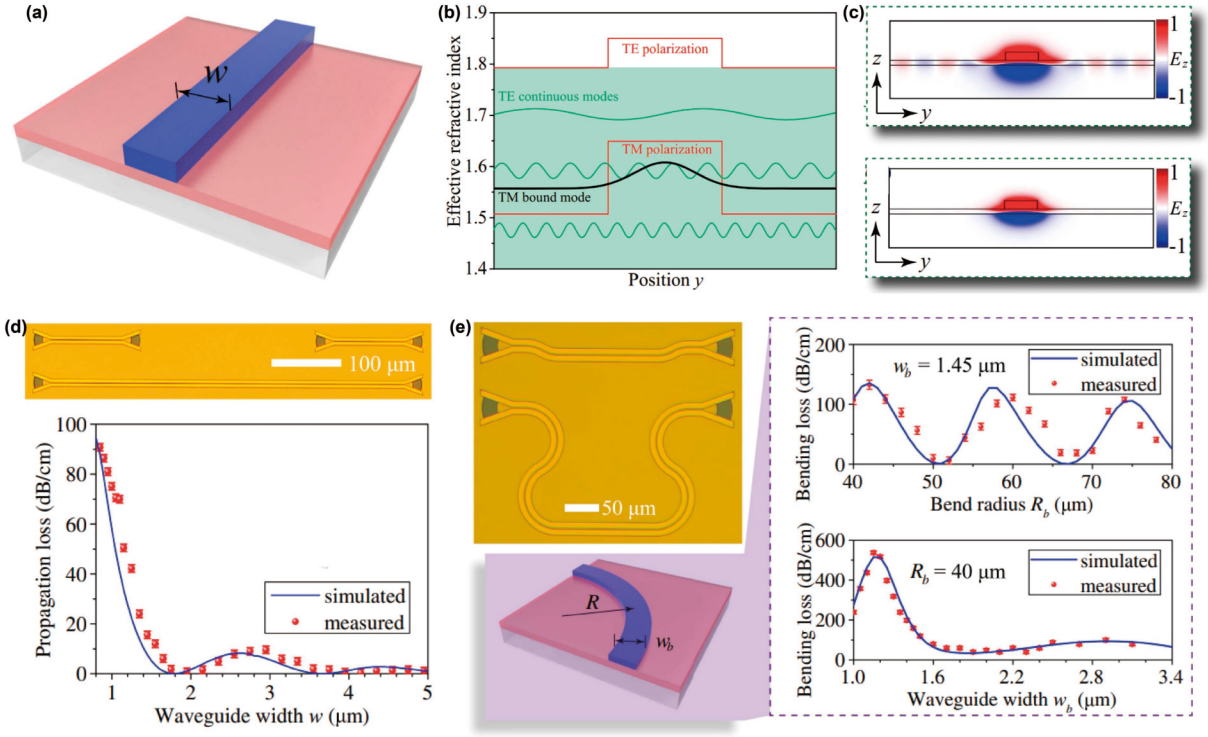

Fig. 6. (Color online) (a) Schematic illustration of a straight hybrid waveguide[56]. (b) RI distributions of *s* and *p* polarizations. (c) Modal profiles of a TM mode in waveguides with BIC and non-BIC parameters[56]. (d) Fabricated straight waveguides and measured propagation loss as a function of waveguide width[56]. (e) Fabricated bent waveguides and measured propagation loss as functions of waveguide width and bending radius[56]. Copyright 2019, The Optical Society.

proved the existence of the BIC. As an application, such a high-quality metagrating is exploited to realize the temperature sensing with a high-temperature sensitivity ≈ 77 pm/K.

A narrowband integrated flat-top filter was proposed by utilizing identical coupled thin-ridge waveguides as shown in Fig. 5(d)[60]. These thin-ridge waveguides operating near a BIC work as a coupled-resonator array for *p*-polarized guided modes, enabling sidelobe-free and flat-top reflectance profiles with steep slopes. Particularly, a two-ridge structure can be seen as a second-order Butterworth filter and an excellent higher-order Butterworth filter can be realized by increasing the number of thin-ridge waveguides. The flat-top reflection band can be an arbitrary value by proper choice of the linewidth of a single-ridge resonance and coupling strength between neighboring ridges. In addition, the linewidth of a single ridge and coupling strength between neighboring ridges can be simply controlled by the width of the ridge and the distance between neighboring ridges.

4. Hybrid waveguides with BICs

Up to now, many excellent materials have been adopted for photonic integration such as silicon, silicon nitride, alumina nitride, lithium niobite ($LiNbO_3$), etc. However, many other materials with excellent properties cannot be utilized due to the lack of high-quality etching. Ordinarily, the material etching process involves chemical reactions so different kinds of materials need to develop different kinds of etching recipes. Therefore, a general method for overcoming the etching challenges of different kinds of materials is highly desired. As shown in Fig. 6(a), a hybrid waveguide with an etching-friendly waveguide atop an etching-challenging dielectric material is a common structure to overcome the etching problem. In order to fully make use of the excellent properties of the dielectric material, the etching-friendly waveguide should have a lower RI than that of the etching-challenging dielectric material so that light can be mainly confined in the dielectric material. However, in this condition, the waveguide is very similar to the case of a ridge waveguide with $n_{sc} < n_{ps}$, e.g., a *s*-polarized RI distribution well is below a TE RI distribution well. Therefore, a TM mode in the TE continuous spectrum should be obtained, then the etching challenge can be solved for different kinds of dielectric materials.

The hybrid waveguide with BICs was first proposed and demonstrated by utilizing a low RI polymer waveguide on a high RI $LiNbO_3$ substrate[56]. Fig. 6(b) plots the RI distributions of a hybrid waveguide with the thicknesses of the $LiNbO_3$ layer of 300 nm at a wavelength of 1550 nm. The modal profiles of the TM modes in waveguides with BIC and non-BIC parameters are shown in Fig. 6(c). Fig 6(d) plots the propagation loss of a straight waveguide as a function of waveguide width, indicating the low-loss TM mode can be obtained by optimizing the waveguide width to BIC parameters. As for a bent waveguide, the propagation loss depends on both the waveguide width and bending radius as shown in Fig. 6(e).

Pivotal photonic components have been demonstrated[56] based on the basic straight and bent waveguides including microcavities, directional couplers, and Mach–Zehnder interferometers (MZIs). The measured transmission spectrum of a microring cavity as shown in Fig. 7(a) indicates that the demonstrated microcavities can support high-*Q* resonances with high extinction ratio over a broad bandwidth of 100 nm. The loaded and intrinsic *Q* factors can reach 2.2×10^5 and 5.8×10^5, respectively. The transmission spectra of a fabri-

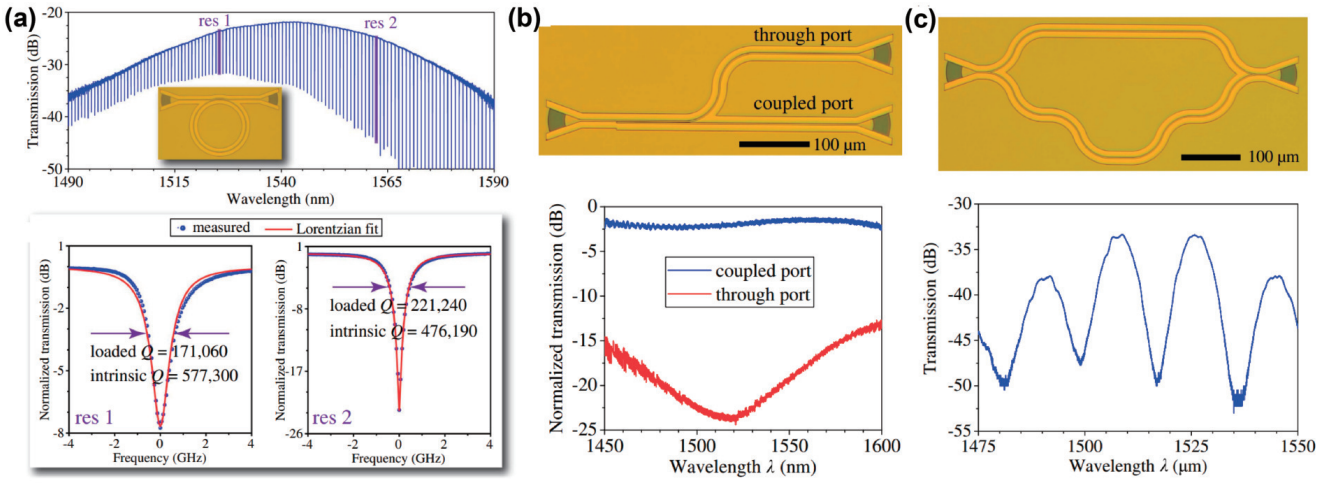

Fig. 7. (Color online) (a) Measured transmission spectrum of the fabricated microring cavity with structural parameters satisfying the BIC condition[56]. (b) Optical microscope image of the fabricated directional coupler and the corresponding measured spectrum[56]. (c) Optical microscope image of the fabricated MZI and the corresponding measured spectrum[56]. Copyright 2019, The Optical Society.

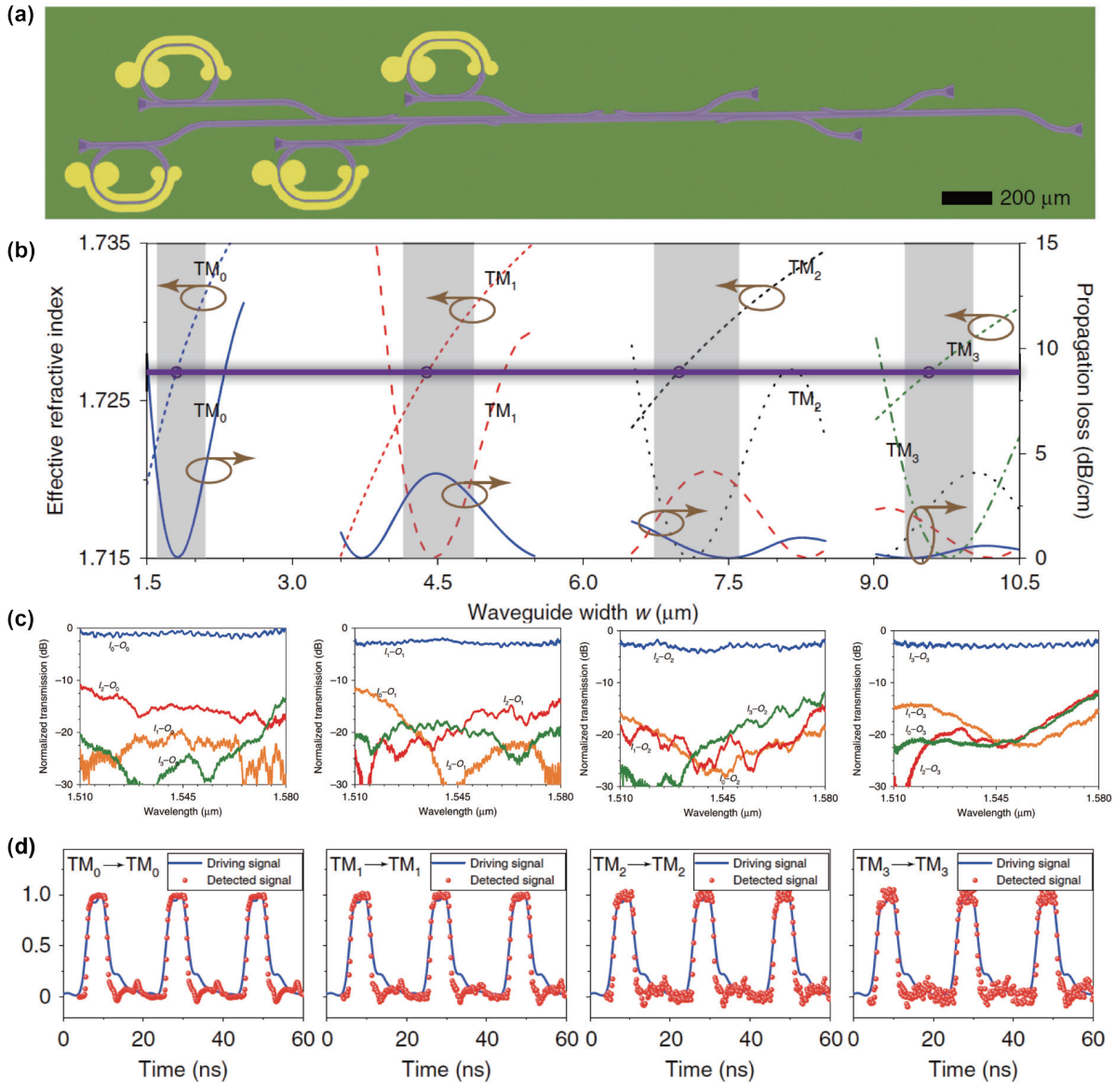

Fig. 8. (Color online) (a) An optical microscope image of the fabricated mode (de)multiplexer integrated with EO modulators[55]. (b) Propagation loss and effective RIs of the different orders of TM modes as a function of the waveguide width w[55]. (c) Normalized spectra of light transmission for a fabricated mode (de)multiplexer[55]. (d) Measured modulated signals for each order of modes[55]. Copyright 2020, Springer Nature Limited.

cated directional coupler as shown in Fig. 7(b) indicate that light can efficiently be coupled from one port to another in the wavelength range of 1450–1600 nm. The measured spectra of the fabricated MZI as shown in Fig. 7(c) has a large extinction ratio, denoting the 3-dB power splitters divide optical power evenly. Moreover, the hybrid waveguide with BICs has also been demonstrated at near-visible wavelength spectrum[84] based on a structure with the thicknesses of the $LiNbO_3$ layer, the buried silicon oxide underneath, and the organic polymer atop are 150 nm, 2 μm, and 500 nm, respectively.

Mode (de)multiplexing. Mode (de)multiplexing is an important freedom among different kinds of (de)multiplexing technologies, which can greatly increase data link capacity to satisfy the huge data transmission requirement. Mode (de)multiplexing and high-dimensional communication were achieved on a $LiNbO_3$ platform utilizing waveguides with BICs as shown in Fig. 8(a)[55], which is composed of several cascaded multimode directional couplers. Fig. 8(b) plots the effective RI and propagation loss of the TM_0 (orange), TM_1 (blue), TM_2 (red), and TM_3 (green) modes as a function of the waveguide width w, indicating the waveguides can be engineered to meet low propagation loss and phase-matching conditions simultaneously. Specifically, the gray areas denote the regions of low propagation loss for the corresponding modes and satisfaction of phase matching can be realized at the intersections of the horizontal solid line and the dashed lines in the gray regions. Fig. 8(c) shows the measured transmission spectra of all pairs of input-output ports. The measured insertion loss (crosstalk) can be <1.7(−14.1), <3.4(−13.8), <4.0(−15.7), and <3.3(−18.5) dB for the TM_0, TM_1, TM_2, and TM_3 modes, respectively, within a wavelength spectrum of 1.51–1.58 μm. Therefore, a hybrid mode–wavelength (de)multiplexing optical network can be constructed to significantly increase optical link capacity based on the wideband mode (de)multiplexer. Furthermore, the capability of on-chip electro-optic (EO) modulation and mode (de)multiplexing simultaneously was evidenced by integrating EO modulators with the mode (de)multiplexer on the same chip. Fig. 8(d) plots the transmission signal for the input and output pairs of TM_0–TM_0, TM_1–TM_1, TM_2–TM_2, and TM_3–TM_3, respectively.

AO modulation. AOs explore phonon–photon coupling based on strain- and stress-induced RI variation in a medium. Brillouin scattering involving the study of propagating phonons is one of the most widely investigated AO effects, which can break the time-reversal and frequency-modulation symmetry of light due to the phase-matching requirement. It has found wide applications in various areas, such as nonreciprocal light transmission[85], modulation[86], frequency shifting[87, 88], and signal processing[89, 90]. AO cavity and waveguide modulations have been demonstrated based on the hybrid waveguides with BICs.

AO cavity modulation has been realized as shown in Fig. 9(a)[59], where a surface acoustic wave (SAW) interdigital transducer (IDT) is monolithically integrated with a photonic microcavity that supports BIC modes on a 400-nm-$LiNbO_3$-on-insulator platform. A SAW will propagate across a BIC waveguide smoothly because the polymer waveguide atop with very different acoustic properties from those of $LiNbO_3$ has a negligible effect on the SAW propagating inside the $LiNbO_3$ thin film. AO modulation with frequency >4 GHz was observed as shown in Fig. 9(b) because of the microscale confinement of SAW. Strong AO coupling, evidenced by induced transparency and absorption as shown in Fig. 9(c), was realized with the assistance of resonant enhancement in the high-Q cavity.

AO waveguide modulation was realized as shown in Fig. 9(d)[61]. The working principle can be described as light input from channel C_1 (C_2) interacts with the counterpropagating (copropagating) traveling SAWs and light scattered to the first order should have a frequency up(down)-shift because of the Doppler effect. The traveling SAWs like a mirror scatter the light beam from the original direction with an angle θ, and thus is deflected into channel C_3 (C_4) for output. The unscattered part of the original light beam keeps its original propagation direction and thus transmits into channel C_4 (C_3). The AO modulation sideband of light is determined by the combinations of input and output channels. Under this scheme, a 3-GHz frequency shifter was achieved as shown in Fig. 9(e), indicating a 3-dB operation bandwidth of ~35 nm. The extinction ratios of the upper(lower)-sideband modulated light to the lower(upper)-sideband modulated and unmodulated light is >44 (47) and 25 (23) dB in the 3-dB operating bandwidth.

2D material integration. Integration of 2D materials on dielectric planar optical waveguides can make available new optoelectronic functionalities from the 2D materials, such as nonlinearity[91], light emission[92], modulation[93], photodetection[14], and saturable absorption[94]. However, the conventional integration schemes involving either the transfer of 2D materials onto prepatterned nonplanarized topology of PICs or the growth and patterning of dielectric materials on 2D materials can degrade the properties of either the dielectric or the 2D material. As shown in Fig. 10(a), a new and practical scheme has been introduced for integrating 2D materials with PICs on a planar surface by using a hybrid waveguide with BICs[63]. This approach applies to the integration of any 2D material on any single-crystal dielectric substrate, and inherently offers strong light–matter interactions. The post waveguide fabrication process will yield negligible effects on 2D materials, which proved that no defect Raman spectra were observed before and after the lithographic patterning when transferring different kinds of 2D materials (graphene, MoS_2, and WS_2) onto different substrates ($LiNbO_3$ and Si_3N_4).

Hybrid integration of graphene on $LiNbO_3$ with BICs was first demonstrated[63]. Various hybrid photonic devices including thermo-optic switches and filters [Fig. 10(b)], high-speed photodetectors [Fig. 10(c)], and EO modulators [Fig. 10(d)] were realized by this approach. For thermo-optic switches and filters, the experimentally measured optical transmission spectra of the fabricated BIC-based microring cavities achieved modulation depths as large as ~35 dB, which are suitable for high-performance optical switches and tunable filters. The measured rise time of the device was as small as ~4.3 μs. For high-speed photodetectors, the responsivity can be as high as 0.4 A/W at a bias voltage of 0.8 V. The measured spectra of the impulse response indicate that the response speed of the graphene photodetector was ~40 GHz. For an EO modulator, the modulation depth of a 100-μm-long modulator was ~3 dB and a modulation bandwidth of ~5 GHz was previously reported.

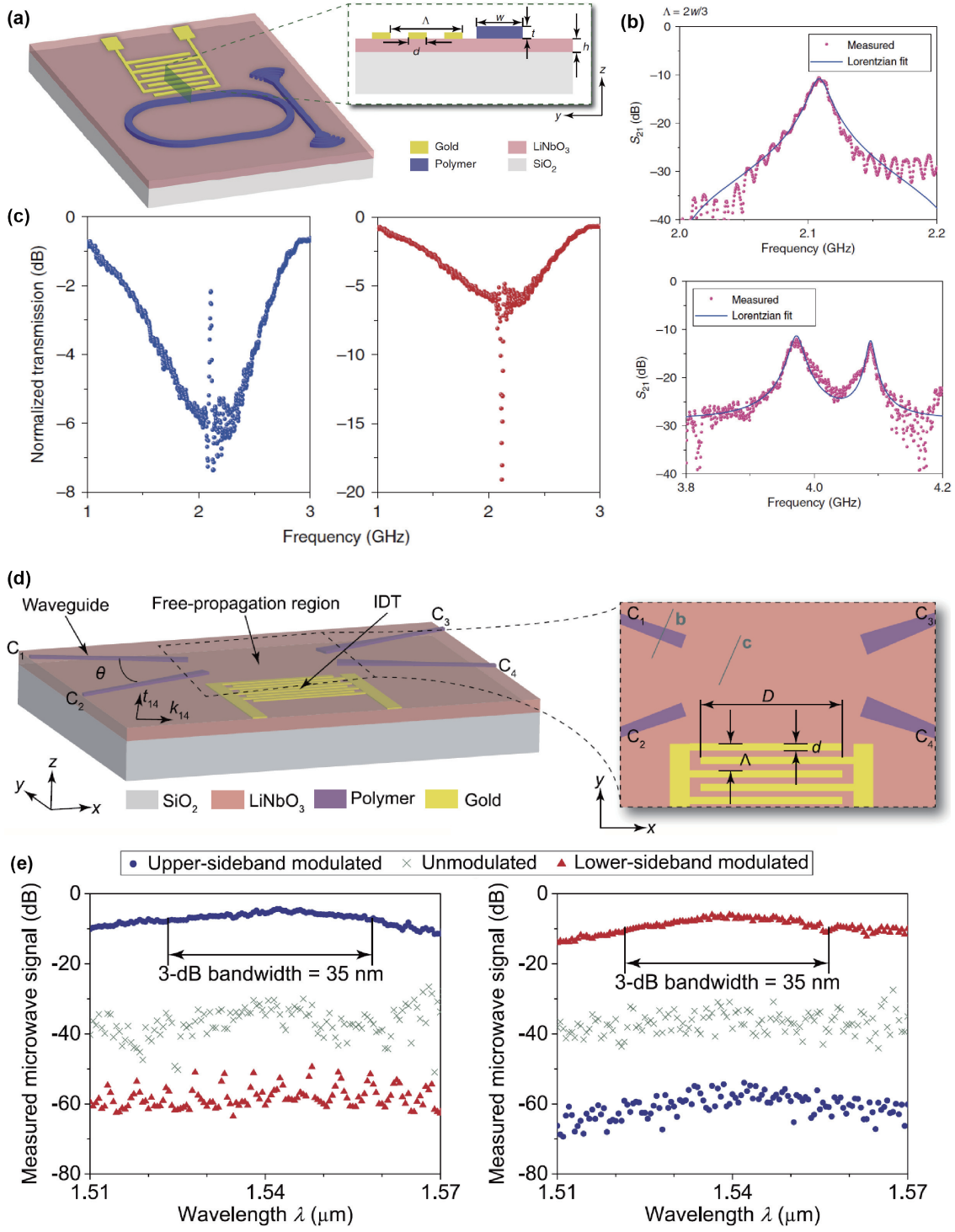

Fig. 9. (Color online) (a) Schematic illustration of AO cavity modulation[59]. (b) Measured AO modulation signals with a frequency higher than 4 GHz[59]. (c) Measured AO-induced transparency and absorption[59]. Copyright 2020, Light: Science & Applications. (d) Schematic illustration of AO waveguide modulation[61]. (e) Measured frequency shifts[61]. Copyright 2021, ACS.

The BIC-based 2D material integration approach has also been utilized in other platforms beyond graphene and $LiNbO_3$. A high-speed hybrid integrated $PtSe_2$ on a Si_3N_4 waveguide photodetector was demonstrated as shown in Fig. 10(e)[62]. Plasmonic structures were used to enhance light–matter interactions and the fabricated $PtSe_2$ waveguide photodetector has a responsivity of ~12 mA/W at a bias voltage of 8 V, but the measured dark current is as low as 317 nA. The optical impulse response measurement yields a 3-dB bandwidth of 35 GHz, demonstrating the potential of this 2D material for high-speed optoelectronic devices.

5. Conclusions

Currently, significant progress has been made for photonic waveguides with BICs, while there are still many challenges and opportunities. The RI contrast of a waveguide for BICs is relatively small, causing large footprints and the limited ability to manipulate light behavior. A convenient polarization rotation structure is highly desired for a pure dielectric waveguide to connect the TE and TM modes because the TE mode has many unique properties that the TM mode does

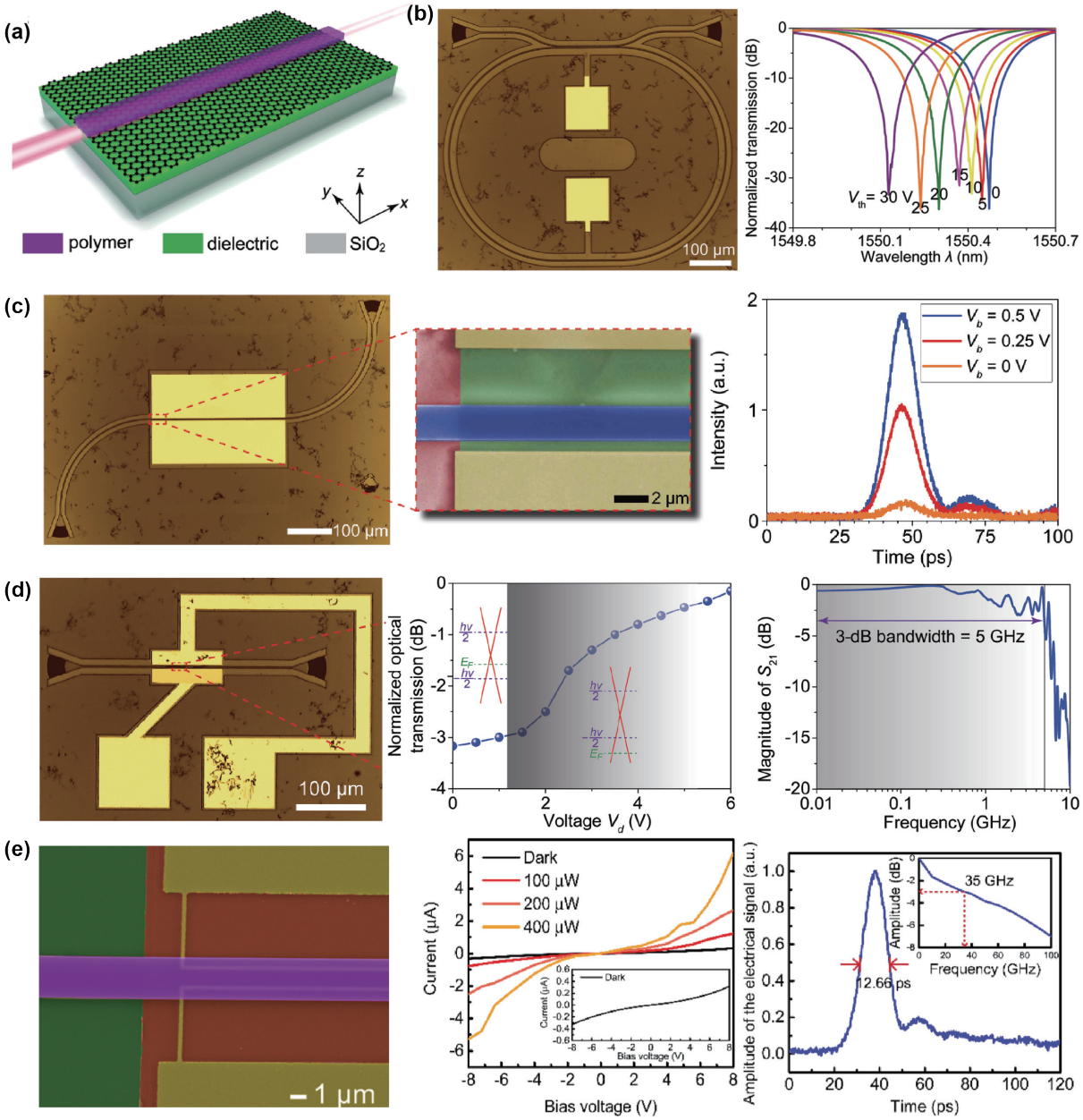

Fig. 10. (Color online) (a) Schematic illustration of a 2D material integrated with a BIC waveguide[63]. (b) A fabricated hybrid graphene thermo-optic modulator with BICs and its measured spectra[63]. (c) A fabricated hybrid graphene photodetector with BICs and its measured optoelectrical response[63]. (d) A fabricated hybrid graphene EO modulation with BIC and its measured EO response[63]. Copyright 2019, John Wiley & Sons. (e) A fabricated hybrid $PtSe_2$ photodetector with BICs and its measured optoelectrical response[62]. Copyright 2020, ACS.

not have. In addition, due to the special coupling behavior between TE and TM modes, PICs with BICs are expected to find applications in polarization manipulation, lateral coupling between well-separated waveguides, and wavelength filtering. Exploring other functional materials with etching problems will also bring many new chances for chip-scale optoelectronic applications. For examples, hybridizing magnetic material like yttrium iron garnet is expected to realize high-performance nonreciprocal devices and strong magnon-optic interaction. Integrating nonlinear material with large Pockels coefficients is highly desired for large-capacity communication, low-threshold wavelength conversion, and efficient microwave-optical conversion.

In conclusion, we have presented an overview of the photonic waveguide with BICs. The fundamentals of these BIC waveguides and the origin of their leakage loss were analyzed in detail. Both pure dielectric (silicon) and hybrid waveguides were discussed. For a silicon waveguide, it can be categorized into two types according to the propagation direction of light, including light propagation along the waveguide and with a certain angle of the waveguide. For a hybrid waveguide, it can be used to construct an etching-free integration platform and different kinds of applications based on the etching-free platform were summarized, including thermo-optic modulation, AO modulation, photodetection, and EO modulation. PICs with BICs are promising in many applications due to their unique mode properties.

Acknowledgement

The authors declare no competing financial interest. Project supported by the National Key Research and Development Program of China (2021YFB2800404), National Natural

Science Foundation of China (62105283), Zhejiang Provincial Natural Science Foundation of China (LDT23F04012F05), and Leading Innovative and Entrepreneur Team Introduction Program of Zhejiang (2021R01001).

References

[1] Thomson D, Zilkie A, Bowers J E, et al. Roadmap on silicon photonics. J Opt, 2016, 18, 073003

[2] Doerr C R. Silicon photonic integration in telecommunications. Front Phys, 2015, 3, 37

[3] Shastri B J, Tait A N, Ferreira de Lima T, et al. Photonics for artificial intelligence and neuromorphic computing. Nat Photonics, 2021, 15, 102

[4] Shen Y C, Harris N C, Skirlo S, et al. Deep learning with coherent nanophotonic circuits. Nat Photonics, 2017, 11, 441

[5] Wang J W, Sciarrino F, Laing A, et al. Integrated photonic quantum technologies. Nat Photonics, 2020, 14, 273

[6] Elshaari A W, Pernice W, Srinivasan K, et al. Hybrid integrated quantum photonic circuits. Nat Photonics, 2020, 14, 285

[7] Liu J Q, Tian H, Lucas E, et al. Monolithic piezoelectric control of soliton microcombs. Nature, 2020, 583, 385

[8] Weimann C, Lauermann M, Hoeller F, et al. Silicon photonic integrated circuit for fast and precise dual-comb distance metrology. Opt Express, 2017, 25, 30091

[9] Lu Y J, Wang C Y, Kim J, et al. All-color plasmonic nanolasers with ultralow thresholds: Autotuning mechanism for single-mode lasing. Nano Lett, 2014, 14, 4381

[10] Liu X F, Zhang Q, Yip J N, et al. Wavelength tunable single nanowire lasers based on surface plasmon polariton enhanced burstein–moss effect. Nano Lett, 2013, 13, 5336

[11] Oulton R F, Sorger V J, Zentgraf T, et al. Plasmon lasers at deep subwavelength scale. Nature, 2009, 461, 629

[12] Grandi S, Nielsen M P, Cambiasso J, et al. Hybrid plasmonic waveguide coupling of photons from a single molecule. APL Photonics, 2019, 4, 086101

[13] Guo J S, Li J, Liu C Y, et al. High-performance silicon–graphene hybrid plasmonic waveguide photodetectors beyond 1.55 μm. Light Sci Appl, 2020, 29, 1

[14] Ding Y H, Cheng Z, Zhu X L, et al. Ultra-compact integrated graphene plasmonic photodetector with bandwidth above 110 GHz. Nanophotonics, 2020, 9, 317

[15] Li Z, Corbett B, Gocalinska A, et al. Direct visualization of phase-matched efficient second harmonic and broadband sum frequency generation in hybrid plasmonic nanostructures. Light Sci Appl, 2020, 9, 180

[16] Agreda A, Sharma D K, Colas des Francs G, et al. Modal and wavelength conversions in plasmonic nanowires. Opt Express, 2021, 29, 15366

[17] Heni W, Haffner C, Elder D L, et al. Nonlinearities of organic electro-optic materials in nanoscale slots and implications for the optimum modulator design. Opt Express, 2017, 25, 2627

[18] Ferrotti T, Blampey B, Jany C, et al. Co-integrated 13μm hybrid III-V/silicon tunable laser and silicon Mach-Zehnder modulator operating at 25Gb/S. Opt Express, 2016, 24, 30379

[19] Zhou J, Huang L J, Fu Z Y, et al. Multiplexed simultaneous high sensitivity sensors with high-order mode based on the integration of photonic crystal 1 × 3 beam splitter and three different single-slot PCNCs. Sensors (Basel), 2016, 16, 1050

[20] Bettotti P. Hybrid materials for integrated photonics. Adv Opt, 2014, 2014, 1

[21] Heni W, Fedoryshyn Y, Baeuerle B, et al. Plasmonic IQ modulators with attojoule per bit electrical energy consumption. Nat Commun, 2019, 10, 1694

[22] Dai D X, Shi Y C, He S L, et al. Gain enhancement in a hybrid plasmonic nano-waveguide with a low-index or high-index gain medium. Opt Express, 2011, 19, 12925

[23] Halir R, Bock P J, Cheben P, et al. Waveguide sub-wavelength structures: A review of principles and applications. Laser Photonics Rev, 2015, 9, 25

[24] Ma J W, Xi X, Sun X K. Topological photonic integrated circuits based on valley kink states. Laser Photonics Rev, 2019, 13, 1900087

[25] Baba T. Slow light in photonic crystals. Nat Photonics, 2008, 2, 465

[26] Iwamoto S, Ota Y, Arakawa Y. Recent progress in topological waveguides and nanocavities in a semiconductor photonic crystal platform. Opt Mater Express, 2021, 11, 319

[27] Ono M, Hata M, Tsunekawa M, et al. Ultrafast and energy-efficient all-optical switching with graphene-loaded deep-subwavelength plasmonic waveguides. Nat Photonics, 2020, 14, 37

[28] Dai D X, He S L. A silicon-based hybrid plasmonic waveguide with a metal cap for a nano-scale light confinement. Opt Express, 2009, 17, 16646

[29] He M B, Xu M Y, Ren Y X, et al. High-performance hybrid silicon and lithium niobate Mach–Zehnder modulators for 100 Gbit s^{-1} and beyond. Nat Photonics, 2019, 13, 359

[30] von Neumann J, Wigner E. On some peculiar discrete eigenvalues. Phys Z, 1929, 30, 465

[31] Hsu C W, Zhen B, Stone A D, et al. Bound states in the continuum. Nat Rev Mater, 2016, 1, 16048

[32] Bulgakov E N, Maksimov D N. Light guiding above the light line in arrays of dielectric nanospheres. Opt Lett, 2016, 41, 3888

[33] Bulgakov E N, Maksimov D N. Topological bound states in the continuum in arrays of dielectric spheres. Phys Rev Lett, 2017, 118, 267401

[34] Bykov D A, Bezus E A, Doskolovich L L. Coupled-wave formalism for bound states in the continuum in guided-mode resonant gratings. Phys Rev A, 2019, 99, 063805

[35] Gomis-Bresco J, Artigas D, Torner L. Anisotropy-induced photonic bound states in the continuum. Nat Photonics, 2017, 11, 232

[36] Hsu C W, Zhen B, Lee J, et al. Observation of trapped light within the radiation continuum. Nature, 2013, 499, 188

[37] Kodigala A, Lepetit T, Gu Q, et al. Lasing action from photonic bound states in continuum. Nature, 2017, 541, 196

[38] Koshelev K, Favraud G, Bogdanov A, et al. Nonradiating photonics with resonant dielectric nanostructures. Nanophotonics, 2019, 8, 725

[39] Longhi S. Optical analog of population trapping in the continuum: Classical and quantum interference effects. Phys Rev A, 2009, 79, 023811

[40] Marinica D C, Borisov A G, Shabanov S V. Bound states in the continuum in photonics. Phys Rev Lett, 2008, 100, 183902

[41] Monticone F, Alù A. Embedded photonic eigenvalues in 3D nanostructures. Phys Rev Lett, 2014, 112, 213903

[42] Plotnik Y, Peleg O, Dreisow F, et al. Experimental observation of optical bound states in the continuum. Phys Rev Lett, 2011, 107, 183901

[43] Rybin M V, Koshelev K L, Sadrieva Z F, et al. High-Q supercavity modes in subwavelength dielectric resonators. Phys Rev Lett, 2017, 119, 243901

[44] Weimann S, Xu Y, Keil R, et al. Compact fano states embedded in the continuum of waveguide arrays. Phys Rev Lett, 2013, 111, 240403

[45] Zhen B, Hsu C W, Lu L, et al. Topological nature of optical bound states in the continuum. Phys Rev Lett, 2014, 113, 257401

[46] Chen Y, Shen Z, Xiong X, et al. Mechanical bound state in the continuum for optomechanical microresonators. New J Phys, 2016, 18, 063031

[47] Hein S, Koch W, Nannen L. Trapped modes and Fano resonances in two-dimensional acoustical duct–cavity systems. J Fluid Mech, 2012, 692, 257

[48] Linton C M, McIver P. Embedded trapped modes in water waves and acoustics. Wave Motion, 2007, 45, 16

[49] Lyapina A, Maksimov D, Pilipchuk A, et al. Bound states in the

continuum in open acoustic resonators. J Fluid Mech, 2015, 780, 370
[50] Xiao Y X, Ma G C, Zhang Z Q, et al. Topological subspace-induced bound state in the continuum. Phys Rev Lett, 2017, 118, 166803
[51] Bulgakov E N, Maksimov D N, Semina P N, et al. Propagating bound states in the continuum in dielectric gratings. J Opt Soc Am B, 2018, 35, 1218
[52] Koshelev K, Lepeshov S, Liu M K, et al. Asymmetric metasurfaces with high-Q resonances governed by bound states in the continuum. Phys Rev Lett, 2018, 121, 193903
[53] Liang Y, Koshelev K, Zhang F C, et al. Bound states in the continuum in anisotropic plasmonic metasurfaces. Nano Lett, 2020, 20, 6351
[54] Bulgakov E N, Sadreev A F. Bloch bound states in the radiation continuum in a periodic array of dielectric rods. Phys Rev A, 2014, 90, 053801
[55] Yu Z J, Tong Y Y, Tsang H K, et al. High-dimensional communication on etchless lithium niobate platform with photonic bound states in the continuum. Nat Commun, 2020, 11, 1
[56] Yu Z J, Xi X, Ma J W, et al. Photonic integrated circuits with bound states in the continuum. Optica, 2019, 6, 1342
[57] Azzam S I, Shalaev V M, Boltasseva A, et al. Formation of bound states in the continuum in hybrid plasmonic-photonic systems. Phys Rev Lett, 2018, 121, 253901
[58] Zou C L, Cui J M, Sun F W, et al. Guiding light through optical bound states in the continuum for ultrahigh-Q microresonators. Laser Photonics Rev, 2015, 9, 114
[59] Yu Z J, Sun X K. Acousto-optic modulation of photonic bound state in the continuum. Light Sci Appl, 2020, 9, 1
[60] Doskolovich L L, Bezus E A, Bykov D A. Integrated flat-top reflection filters operating near bound states in the continuum. Photon Res, 2019, 7, 1314
[61] Yu Z J, Sun X K. Gigahertz acousto-optic modulation and frequency shifting on etchless lithium niobate integrated platform. ACS Photonics, 2021, 8, 798
[62] Wang Y, Yu Z J, Zhang Z Y, et al. Bound-states-in-continuum hybrid integration of 2D platinum diselenide on silicon nitride for high-speed photodetectors. ACS Photonics, 2020, 7, 2643
[63] Yu Z J, Wang Y, Sun B L, et al. Hybrid 2D-material photonics with bound states in the continuum. Adv Optical Mater, 2019, 7, 1901306
[64] Dalvand N, Nguyen T G, Koch T L, et al. Thin shallow-ridge silicon-on-insulator waveguide transitions and tapers. IEEE Photonics Technol Lett, 2013, 25, 163
[65] Dalvand N, Nguyen T G, Tummidi R S, et al. Transition from "magic width" to "anti-magic width" in thin-ridge silicon-on-insulator waveguides. 2012 Conference on Lasers and Electro-Optics (CLEO), San Jose, CA, USA, 2012, 1
[66] Hope A P, Nguyen T G, Mitchell A, et al. Quantitative analysis of TM lateral leakage in foundry fabricated silicon rib waveguides. IEEE Photonics Technol Lett, 2016, 28, 493
[67] Webster M A, Pafchek R M, Mitchell A, et al. Width dependence of inherent TM-mode lateral leakage loss in silicon-on-insulator ridge waveguides. IEEE Photonics Technol Lett, 2007, 19, 429
[68] Koshiba M, Kakihara K, Saitoh K. Reduced lateral leakage losses of TM-like modes in silicon-on-insulator ridge waveguides. Opt Lett, 2008, 33, 2008
[69] Xu X J, Chen S W, Yu J Z, et al. An investigation of the mode characteristics of SOI submicron rib waveguides using the film mode matching method. J Opt A: Pure Appl Opt, 2009, 11, 015508
[70] Ako T, Hope A, Nguyen T, et al. Electrically tuneable lateral leakage loss in liquid crystal clad shallow-etched silicon waveguides. Opt Express, 2015, 23, 2846
[71] Kakihara K, Saitoh K, Koshiba M. Generalized simple theory for estimating lateral leakage loss behavior in silicon-on-insulator ridge waveguides. J Light Technol, 2009, 27, 5492
[72] Nguyen T G, Tummidi R S, Koch T L, et al. Rigorous modeling of lateral leakage loss in SOI thin-ridge waveguides and couplers. IEEE Photonics Technol Lett, 2009, 21, 486
[73] Ako T, Beeckman J, Bogaerts W, et al. Tuning the lateral leakage loss of TM-like modes in shallow-etched waveguides using liquid crystals. Appl Opt, 2014, 53, 214
[74] Nguyen T G, Tummidi R S, Koch T L, et al. Lateral leakage in TM-like whispering gallery mode of thin-ridge silicon-on-insulator disk resonators. Opt Lett, 2009, 34, 980
[75] Dalvand N, Nguyen T G, Tummidi R S, et al. Thin-ridge silicon-on-insulator waveguides with directional control of lateral leakage radiation. Opt Express, 2011, 19, 5635
[76] Nguyen T G, Ren G H, Schoenhardt S, et al. Ridge resonance in silicon photonics harnessing bound states in the continuum. Laser Photonics Rev, 2019, 13, 1900035
[77] Bezus E A, Bykov D A, Doskolovich L L. Bound states in the continuum and high-Q resonances supported by a dielectric ridge on a slab waveguide. Photon Res, 2018, 6, 1084
[78] Hammer M, Ebers L, Förstner J. Oblique evanescent excitation of a dielectric strip: A model resonator with an open optical cavity of unlimited Q. Opt Express, 2019, 27, 9313
[79] Peng S T, Oliner A A. Guidance and leakage properties of a class of open dielectric waveguides: Part I - mathematical formulations. IEEE Trans Microw Theory Tech, 1981, 29, 843
[80] Muellner, P., N. Finger, and R. Hainberger. Lateral leakage in symmetric SOI rib-type slot waveguides. Optics Express, 2008, 16(1): p.287–294.
[81] Nguyen T G, Tummidi R S, Koch T L, et al. Lateral leakage of TM-like mode in thin-ridge silicon-on-insulator bent waveguides and ring resonators. Opt Express, 2010, 18, 7243
[82] Dai D X, Wang Z, Julian N, et al. Compact broadband polarizer based on shallowly-etched silicon-on-insulator ridge optical waveguides. Opt Express, 2010, 18, 27404
[83] Xu H N, Shi Y C. Silicon-waveguide-integrated high-quality metagrating supporting bound state in the continuum. Laser Photonics Rev, 2020, 14, 1900430
[84] Yu Y, Yu Z J, Wang L, et al. Ultralow-loss etchless lithium niobate integrated photonics at near-visible wavelengths. Adv Optical Mater, 2021, 9, 2100060
[85] Sohn D B, Kim S, Bahl G. Time-reversal symmetry breaking with acoustic pumping of nanophotonic circuits. Nat Photonics, 2018, 12, 91
[86] Gavartin E, Verlot P, Kippenberg T J. A hybrid on-chip optomechanical transducer for ultrasensitive force measurements. Nat Nanotechnol, 2012, 7, 509
[87] Beugnot J C, Lebrun S, Pauliat G, et al. Brillouin light scattering from surface acoustic waves in a subwavelength-diameter optical fibre. Nat Commun, 2014, 5, 1
[88] Chan E H W, Minasian R A. All-optical frequency shifter based on stimulated Brillouin scattering in an optical fiber. IEEE Photonics J, 2014, 6, 1
[89] Kang M S, Butsch A, St J Russell P. Reconfigurable light-driven opto-acoustic isolators in photonic crystal fibre. Nat Photonics, 2011, 5, 549
[90] Santagiustina M, Chin S, Primerov N, et al. All-optical signal processing using dynamic Brillouin gratings. Sci Rep, 2013, 3, 1594
[91] Alexander K, Savostianova N A, Mikhailov S A, et al. Electrically tunable optical nonlinearities in graphene-covered SiN waveguides characterized by four-wave mixing. ACS Photonics, 2017, 4, 3039
[92] Ge X C, Minkov M, Fan S H, et al. Laterally confined photonic crystal surface emitting laser incorporating monolayer tungsten disulfide. Npj 2D Mater Appl, 2019, 3, 1
[93] Phare C T, Lee Y H D, Cardenas J, et al. Graphene electro-optic modulator with 30 GHz bandwidth. Nat Photonics, 2015, 9, 511
[94] Li Z Q, Dong N N, Zhang Y X, et al. Invited article: Mode-locked waveguide lasers modulated by rhenium diselenide as a new saturable absorber. APL Photonics, 2018, 3, 080802

Zejie Yu received the B.E. degree in Optical Engineering from Zhejiang University and the Ph.D. degree in Electronic Engineering from The Chinese University of Hong Kong. Later he was a Postdoctoral Scholar at the Department of Electronic Engineering, The Chinese University of Hong Kong. He is currently a tenure-track Professor with the College of Optical Science and Engineering, Zhejiang University. His research interests include silicon photonics and heterogeneous integration.

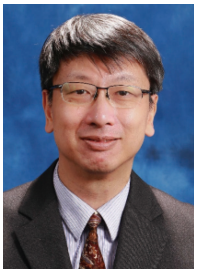

Hon Ki Tsang (Fellow, IEEE) received the B.A. (Hons.) and Ph.D. degrees from the University of Cambridge, Cambridge, U.K., in 1987 and 1991, respectively. He joined The Chinese University of Hong Kong, Hong Kong, in 1993 and was the Chairman of the Department of Electronic Engineering during 2010–2016. He is currently an Associate Dean (Research) of the Faculty of Engineering. He has coauthored more than 400 papers in journals and conference proceedings. His research interests include photonic integrated circuits, silicon photonics, nonlinear waveguides, hybrid integration of two-dimensional materials, optical communications, and integrated quantum photonics. He is currently the Editor-in-Chief of the IEEE Journal of Quantum Electronics.